

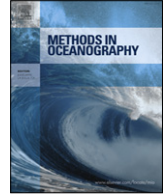


ELSEVIER

Contents lists available at ScienceDirect

Methods in Oceanography

journal homepage: www.elsevier.com/locate/mio



Full length article

On the use of high-frequency broadband sonar to classify biological scattering layers from a cabled observatory in Saanich Inlet, British Columbia



Tetjana Ross^{a,*}, Julie E. Keister^b, Ana Lara-Lopez^c

^a Department of Oceanography, Dalhousie University, Halifax NS B3H 4R2, Canada

^b School of Oceanography, University of Washington, United States

^c Scripps Institution of Oceanography, United States

ARTICLE INFO

Article history:

Received 15 June 2012

Received in revised form

24 April 2013

Accepted 23 May 2013

Available online 26 July 2013

Keywords:

Ocean observatories

Acoustic methods

Zooplankton

Classification

Broadband acoustics

ABSTRACT

This paper explores the use of broadband acoustics to differentiate between biological scattering layers using observatory-based acoustic observations with minimal supporting biological observations. Targets and layer assemblages were classified based on 85–155 kHz acoustic data collected on the VENUS observatory in Saanich Inlet, B.C. between March 2008 and February 2010 using a clustering algorithm and different broadband acoustic data descriptors. First, a 6-h segment of data, for which there were coincident depth-resolved net-tow data, was analyzed. Clustering based on the calibrated spectrum of volume scattering strength for each target resulted in clusters that were distributed just as those resulting from clustering based on 120 kHz narrowband data because the clustering was dominated by the scattering level, rather than the spectral shape. When the target spectra were normalized, the clustering results were consistent with the different taxa found in the net samples, but often could not distinguish taxonomic groups. However, layers with distinct species assemblages had different distributions of target classifications, suggesting the assemblages could be distinguished using frequency-dependent scattering information. Ensemble-averaging the scattering observations and converting the spectral data to a 3-descriptor acoustic color representation prior to clustering was (1) more effective

* Corresponding author.

E-mail address: tetjana@dal.ca (T. Ross).

at distinguishing the dominant scattering layers based on their assemblages and (2) much more efficient in terms of computational cost. Clustering two years of acoustic-color data identified 4 main groups (diel migrating euphausiids and chaetognaths, fish, and a mix of pteropods and bottom-to-oxycline migrating amphipods) that were consistent with contemporaneous and historical observations of zooplankton in the inlet. A wider frequency band might be effective in better distinguishing individual zooplankton targets.

© 2013 Elsevier B.V. All rights reserved.

1. Introduction

High-frequency acoustic observations, each ping rich in information on the whole water column, are ideally suited to long-term deployment on cabled ocean observatories. High-frequency acoustics can provide high-resolution, long-term records of fine-scale vertical distribution and abundance of zooplankton and other marine organisms in the ocean. On cabled observatories, long-term acoustic records are no longer limited by data storage or power (Dewey et al., 2009), leading to unprecedented ability to perform longitudinal studies (e.g. inter-annual variability in zooplankton populations). However, work remains to be done to develop reliable target and layer discrimination and classification algorithms (Horne, 2000). Accurately discriminating and classifying targets and layers composed of a mixture of targets is critical for ecological (e.g. interaction within or between different trophic levels) and fisheries (e.g. stock assessment) studies (Trenkel et al., 2011).

The information in acoustic scattering signals that allows target discrimination is largely frequency dependent. This has led to studies using multi-frequency (e.g. Horne, 2000; Warren et al., 2003) and broadband (e.g. Lavery et al., 2010; Stanton et al., 2010) acoustic data, along with other environmental data, to infer species composition. Broadband data have the added benefit of improved spatial resolution, allowing better target isolation and noise suppression through the use of pulse compression techniques (Chu and Stanton, 1998). Broadband measurements and theoretical physics-based approaches for classifying zooplankton have been combined successfully (Stanton et al., 1998; Roberts and Jaffe, 2007, 2008) in the laboratory. Field-applicable broadband target discrimination and classification techniques, however, are still in the early stages of development (e.g. Stanton et al., 2010). Ground-truth information remains critical for accurately estimating the abundance and composition of acoustically-observed animal aggregations (Holliday, 1977; Greenlaw, 1979; Lawson et al., 2008).

Acoustic datasets, and particularly broadband datasets, collected during ship-based surveys or from a moored instrument can be enormous. Automated or semi-automated classification techniques can be very useful in managing and interpreting this acoustic information. Cluster analysis has been used effectively to classify fish, based on both school properties (e.g. Burgos and Horne, 2008) and frequency dependence (e.g. Anderson et al., 2007), as well as krill swarms (e.g. Cox et al., 2011; Tarling et al., 2009) and seabed type (e.g. Preston, 2009). Clustering, or another blind classification scheme (i.e. one that is not trained based on some supporting dataset), is well suited to datasets where the supporting biological observations are sparse and likely not representative of all the species present throughout the observation period. This limitation due to insufficient supporting data is certainly present in the 'typical' observatory-based acoustic dataset. Combining this with the fact that no hierarchical relationships are expected between the zooplankton groups, it is likely that simple non-hierarchical, blind classification techniques are likely to be the most useful in the automation of the identification of zooplankton layer in mooring-based acoustic observations.

One of the biggest difficulties in applying clustering techniques to acoustic data is choosing what variables or descriptors of each data point to include as dimensions in the multidimensional space in which the clustering algorithm operates. Broadband acoustic data offers a means of distinguishing between different types of scatterers based on their scattering spectra (e.g. Lavery et al., 2010; Stanton

et al., 2010). Scattering spectra may, therefore, be an effective descriptor for classification of scattering targets and/or layers using clustering techniques.

This paper explores the effectiveness of using scattering spectra from a broadband acoustic mooring to classify observed scattering layers. We use data from a 85–155 kHz upward-looking sonar deployed in Saanich Inlet, B.C. from March 2008 through February 2010. Coincident zooplankton net samples were collected on July 30, 2009. First, *k*-means clustering was applied to a subset of data from July 30, 2009 to explore the effectiveness of automatic classification based on different types of descriptors derived exclusively from acoustic scattering data. Using the net-tow data for comparison, we consider whether data from a single broadband transducer provides sufficient power for classification and whether the large volumes of data collected by broadband transducers can be simplified while still effectively discriminating among distinct scattering layers. Second, simplified and more computationally-efficient data descriptors are used to cluster the entire two-year acoustic record; results are described in relation to what is known about the resident species assemblage and behavior.

2. Experimental location

Saanich Inlet is a 24-km long fjord with mid-basin depths around 230 m that is separated from the Strait of Georgia by a 75 m sill. It is a relatively simple oceanographic environment: there is little freshwater run-off entering the inlet, currents are weak, and an anoxic layer is often present below the depth of the sill (Herlinveaux, 1962; Gargett et al., 2003). The anoxic layer is only flushed about once per year (Anderson and Devol, 1973; Gargett et al., 2003). The presence of this persistent deep anoxic layer affects the zooplankton ecology in the inlet (e.g. Boden and Kampa, 1965; De Robertis et al., 2001). Multiple studies, including acoustic, optical and net data, have shown that a very strong daytime scattering layer at the upper edge of the anoxic layer is composed primarily of euphausiids (mainly *Euphausia pacifica*) and amphipods (mainly *Ochomenella* spp.) (e.g. Bary et al., 1962). The amphipods feed on the bottom and migrate to the edge of the oxic layer to respire (De Robertis et al., 2001). Euphausiids aggregate, sometimes at astonishing densities (up to 10 000/m³ over 2 to 3 m; Mackie and Mills, 1983), just above the anoxic layer during the day and migrate to the surface to feed at night (e.g. De Robertis et al., 2000). The relatively low species richness in these dense zooplankton aggregations (Bary et al., 1962; De Robertis et al., 2000) has made it a popular site for acoustic experiments. Multi-frequency techniques, when the scattering layer was dominated by euphausiids, have predicted size class structure and concentrations consistent with historical and concurrent observations (e.g. Greenlaw, 1979; Romaine et al., 2002). The low species richness reduces the uncertainty and complexity in interpreting and classifying broadband backscattering data.

3. Methods

3.1. Broadband sonar

Acoustic data were collected with a bottom-mounted upward-looking 85–155 kHz broadband echosounder deployed from March 2008 to Feb 2010 at about 100 m depth on the Saanich Inlet (British Columbia) node of the VENUS observatory (Dewey et al., 2009). The broadband sonar system, a modification of the commercial SciFish Model 2100 system (Brundage and Jung, 2009), transmitted using a single broadband transducer with center frequency of 120 kHz and a 70 kHz band. The transducer had an approximately conical beam-pattern with the full beamwidth ranging from about 16° at 85 kHz to 8.5° at 155 kHz. When in operation on the mooring, the sonar transmitted linear frequency-modulated pulses, spanning 85–155 kHz, 1 ms in duration, once per second, usually at the maximum power setting (524 $V_{\text{peak-to-peak}}$). After each pulse, the received voltage was logged with a constant gain (generally the maximum allowable by the system) at a sampling rate of 500 kHz for 65 536 samples (or 0.1311 s) giving a range of about 97 m. The system collected echo data from 3 m above the bottom to a few meters below the surface (1–6 m, depending on the deployment depth and the phase of the tide). These data were stored on a computer housed in the sonar pressure case and uploaded in near real-time. While the cabled mooring allows Ethernet access to the sonar in real-time, the great volume of data meant that it was not possible to run the sonar while uploading data.

Table 1

Details of broadband sonar deployment on VENUS observatory in Saanich Inlet, British Columbia.

Start	End	Lat [N]	Long [W]	Depth [m]	Comments
2008-03-01	2008-09-27	48° 39.0532	123° 29.2435	100	Maximum transmit power (524V _{pp})
2008-09-28	2009-02-12	48° 39.0829	123° 29.2069	99	Reduced transmit power (142, 182V _{pp})
2009-02-16	2009-09-26	48° 39.0469	123° 29.2410	102	Maximum transmit power (524V _{pp})
2009-09-30	2010-02-17	48° 39.0505	123° 29.2486	102.5	Maximum transmit power (524V _{pp}), Calibration data collected at all transmit powers

Consequently, the sonar was generally operated continuously for about a week, interrupted by 1 to 2 days without observations while the data were uploaded.

Every six months, the sonar was retrieved and redeployed during regular maintenance to the VENUS node instrument package. In addition to slight changes in location and depth (given in Table 1), during the second deployment the transmit power had to be reduced to minimize interference with a nearby sonar operating at 200 kHz.

3.1.1. Pulse compression and scattering spectra

The received voltages were pulse compressed, that is the envelope of the scaled cross-correlation between the transmitted and received signals for each ping was calculated to improve the range resolution and signal-to-noise ratio (Chu and Stanton, 1998; Stanton and Chu, 2008). Since it was not possible to collect a sample of the transmitted pulse *in situ* and the monostatic system started recording 100 μ s before the pulse was transmitted, the first 0.1–1.1 ms of each ping was used in the cross-correlation with the received signal.

To calculate volume scattering strength (following Lavery et al., 2010; Stanton et al., 2010), each pulse compressed ping was split into 512-point (about 1 ms or 75 cm range) segments and the Fourier transform (FT) was calculated. Then these spectra were corrected for spherical spreading and absorption and then divided by the beam's sampling volume at that range (using the factory measured full beamwidth at -3 dB for each frequency). The base-ten logarithm of these spectra were then converted to volume scattering strength (S_V in units of dB re m^{-1}) using a frequency-dependent calibration coefficient derived from a standard target calibration (see 3.1.2). For the acoustic color analysis (Section 3.1.3), these individual-ping spectra were incoherently ensemble-averaged (the number of pings averaged will be provided as appropriate) to produce the S_V for each range bin.

Because the transmitted signal was so much larger than the received signal and the dynamic range of the SciFish system was only about 45 dB, the transmit portion used in the pulse compression was extremely clipped at all the gain and power settings. The clipped amplitude was between 0.003% (for highest power and gain settings) and 0.1% (for lowest power and gain settings) of the nominal amplitude it would have had if it had not been clipped. Ideally one would use a non-clipped version of the transmitted pulse to do pulse compression, so a synthetic test of the sensitivity of the pulse compression method to the use of a very clipped pulse was performed. To do this, first a transmit pulse was created, using a 1 ms 85–155 kHz chirp pulse that had a smoothly varying envelope ramping up and down within 0.2 ms with a small undulation in amplitude in between. The received signal was then created by assuming a perfect reflection on a background of Gaussian noise of about 20% the amplitude of the reflection; that is adding the transmit pulse half-way through a time series of random noise.

3.1.2. Acoustic calibration

On the final 6-month deployment of the sonar, a 1.6 cm tungsten-carbide sphere was floated in the far-field of the transducer in order to perform an *in situ* standard target calibration. Due to the difficulty in deploying the instrument package with lines floating in the water, this was done by attaching a small canister to the edge of the sonar's pressure case. Monofilament line was coiled within the

canister, with one end attached to the bottom of the canister and the other end attached to a lid made out of syntactic foam. When the links securing the lid dissolved, it floated up, pulling the target sphere into the beam of the transducer. The foam was at 3 m range and the sphere at 2.5 m range, putting them in the far field with sufficient separation that their reflections were easily distinguished in the pulse compressed data.

The frequency-dependent target strength of the 1.6 cm tungsten-carbide sphere, modeled as a solid homogeneous elastic sphere (Faran, 1951), undulated smoothly between -50 and -47 dB re m^2 in the frequency range of our broadband system. With no resonances to deal with, a simple standard-target calibration (e.g. Vagle et al., 1996) was performed on a frequency by frequency basis. During the Sept. 2009 to Feb. 2010 deployment, the sphere was constantly in the beam of the sonar. However, with the settings used throughout most of the 2-year deployment (i.e. maximum power and gain) the returns from the sphere were clipped. In order to test linearity of the system (and accuracy of the settings), between Dec. 15 to 17, 2009 the sonar was operated at all combinations of power and gain where the sphere return was not clipped, which includes both maximum power and maximum gain but not together. For all 30-ping ensemble-averages of these calibration runs that were not clipped and were also above the noise-floor of the system, an uncalibrated target strength spectrum was calculated using the method outlined above for volume scattering strength using ten-ping averages, but without correcting for sampling volume. The target strength spectra were converted to the equivalent uncalibrated spectra for full power and full gain based on the nominal power and gain settings. The majority of non-clipped spectra (both high power and low gain and low power and high gain) agreed in shape and, while there was variability in the scattering levels, there was no trend with settings once normalized. Thus, the nominal settings were considered accurate and all spectra were pooled.

There were several outlier spectra, which were identified by looking at the time series of the mean spectral level and rejecting spectra which had a mean level of more than 8 times their neighbors. In all, less than 0.5% were excluded from the pool as outliers and this removed all of the spectra with unusual shapes. Of the remaining 10 206 pooled observations, the 10% with maximum return strength were averaged in linear-space, based on the assumption that the sphere moved in and out of the center of the beam and was centered at least 10% of the time. The difference between this average spectrum and the theoretical target strength spectrum, i.e. the frequency-dependent calibration coefficient, was used to convert all other spectra into units of volume scattering strength. While the assumption of 10% was somewhat arbitrary, the resulting calibration coefficient was not particularly sensitive to the choice. Choosing any value between 1% and 30% yielded a calibration coefficient within 1 dB (on average) of the one used.

3.1.3. Acoustic color

Working with pulse compressed data and their spectra involves manipulating huge datasets [O(10 000) points per ping], which can be impractical for long time series. An alternate approach, which reduces the volume of data by an order of magnitude or more while retaining some frequency-dependent scattering information, is to convert the data into acoustic color images (Miklovic and Bird, 1998; Intrator et al., 2004). With the exception of some noise peaks, the scattering spectra observed in Saanich Inlet generally varied smoothly over the 85–155 kHz frequency range. A particularly large noise peak at 106 kHz (insensitive to water column conditions) was removed by replacing the scattering strengths between 100.5 and 110.5 kHz with the average of the values in the adjacent uncontaminated frequency bins. The S_V values were also thresholded to remove those with low signal-to-noise-ratio (SNR). Using records of at least 24 h length to ensure that noise was observed at each range, the range-dependent noise was estimated as the minimum value observed at each range. Any S_V value that was within 10 dB of the noise level for that range bin was removed from analysis.

For each scattering observation, its 85–155 kHz backscattering spectrum was mapped into the three color channels of a red–green–blue (R–G–B) image as follows. First, the volume scattering strength at each frequency was thresholded between -40 and -80 dB. These limits were chosen because the noise floor was approximately -80 dB at long ranges (i.e., 90–100 m) and less than 2% of the observed S_V exceeded -40 dB in our dataset. Each S_V spectrum was then linearly interpolated onto an axis that ran between 0 and 1, with $S_V \geq -40 \rightarrow 1$ and $S_V \leq -80 \rightarrow 0$. The resultant value

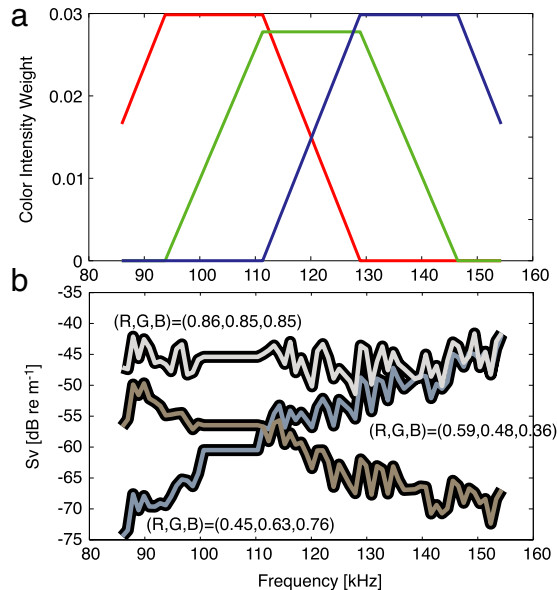


Fig. 1. Illustration of the acoustic color method. (a) Plot of the weighting functions used to map the full 85–155 kHz spectra calculated from the SciFish pings into a red (R), green (G), and blue (B) colors. Each curve sums to 1. Note that the weights taper off in the 85–90 and 150–155 kHz ranges because the transducer is less sensitive at the edge of its usable band. (b) Three example spectra from targets in the July 30, 2009 data, plotted in the color and intensity resulting from the acoustic color method (surrounded by black lines to enhance visibility). The weighting shown in (a) was used along with the intensity limits: $(0, 0, 0) \leq -80$ dB across the band and $(1, 1, 1) \geq -40$ dB across the band.

at each frequency was then multiplied by each of the three color functions plotted in the top panel of Fig. 1. This corresponds to mapping to a colorscale that runs linearly between red, green and blue and is weighted such that the sum across the 85–155 kHz band is exactly one for each color channel. The values in each color channel were then summed across the frequencies to give the R–G–B color triplet for that scattering observation. Scattering observations which were below the -80 dB threshold in all frequency bands would result in black $(0, 0, 0)$ whereas those with ≥ -40 dB intensity across all bands would result in white $(1, 1, 1)$. The procedure reduces the quantity of data by a factor of $N_f/3$, where N_f is the number of frequencies (typically $O(100)$), while retaining some information on the shape of the spectra across the 85–155 kHz band.

3.2. Clustering technique

The goal of cluster analysis is to partition a set of observations into several groups in which the within-group differences are minimized and the between-group differences are maximized. In this study, we used the k -means algorithm (MacQueen, 1967; Gan et al., 2007), one of the most commonly used clustering techniques and an example of a non-hierarchical, blind classification technique. We chose it for its computational simplicity, which is an advantage when working with large datasets, and for its conceptual simplicity, an advantage for this study which aims to demonstrate the general use of data reduction and clustering to aid the interpretation of broadband sonar observations collected from ocean observatories. Possibly the biggest disadvantage of k -means clustering for this study is that it is a type of exclusive clustering which attempts to force clusters of identical size. Hierarchical and probabilistic clustering techniques relax that restriction but have underlying assumptions that we considered potentially inappropriate for our data.

In k -means clustering, n observations are partitioned into k clusters, with k corresponding centroids. For any observation in a given cluster, the distance between this observation and its cluster

centroid should be smaller than the distance between this observation to other cluster centroids. In a multidimensional space, the distance between two points can be calculated many ways. This study used the Manhattan (or city block) distance measure (Gan et al., 2007). The clustering was initialized by randomly assigning k observations as the centroids for k clusters (with the number k chosen as described below), then observations were iteratively associated with the closest cluster and new centroids defined until the centroids converged to a stable set of locations. In order to minimize sensitivity to the initial positions of the centroids, which can lead to convergence to a local rather than global minimum, 5 replicates were performed with different initial centroids chosen at random from the data. Five replicates were performed because (1) five was the minimum number where the majority converged to the same minimum and (2) there was a desire to minimize computational time.

The number of clusters, k , was chosen using a variant of the elbow method (e.g. Friedman and Rubin, 1967), which looks for the start of a plateau in a plot of variance explained versus number of clusters. The k -means clustering technique was applied successively with $k = (2, 3, 4, \dots)$ and the ratio of the mean between cluster least-squares scatter to the total least-squares scatter was tracked (Friedman and Rubin, 1967). This ratio increases with increasing k until the clusters are not sufficiently differentiated. When the ratio increased by less than 10% with the addition of the m th cluster, $m - 1$ clusters was taken as optimal.

3.2.1. Clustering of targets

With the idea that different targets may occupy different depths at different times while retaining a consistent and distinct spectral shape, broadband spectra derived from individual targets were used as descriptors in the clustering analysis. Because of the large volume of data, the analysis was restricted to July 30, 2009, 18:00–24:00 (PDT), when the net tows were conducted. Taking advantage of the full spatial resolution of the broadband data, peaks in compressed pulse output were used to precisely locate individual targets, or groups of targets that were not individually resolvable, within a single ping. This was done on every tenth ping, because this provided sufficient temporal resolution and reduced the computational time significantly. The echo time series of each ping was divided into constant-length segments of the chosen FT size. The segments in which at least one compressed pulse output peak exceeded the chosen threshold were selected for clustering analysis. The threshold was chosen so that the segments' backscattering signals were well above noise; the threshold was 0.08 in the units of the compressed pulse output, which resulted in the retention of only targets with a mean S_V of at least -70 dB, which was about 10 dB above the noise floor at long ranges (-80 dB). Each selected segment was tagged with a single (i.e. not averaged) spectrum of volume scattering strength (calculated as described in Section 3.1.1). So far this follows the procedure of Lee (2009), who then clustered the data based on the coefficients of polynomial fits to normalized, but uncalibrated spectra. Here, we have calibrated spectra of S_V , with a frequency resolution of approximately 1 kHz between 85 and 155 kHz, that can be used as a 71-point descriptor of each scattering observation. To compare the results of clustering based on spectral (i.e. broadband) versus single-frequency (i.e. narrowband) descriptors, the clustering analysis was done three ways. First using the calibrated broadband spectra as 71-dimensional descriptors, second using the calibrated volume scattering strength at 120 kHz as 1-dimensional descriptors and, finally, normalizing the broadband spectra by subtracting the maximum S_V from each spectrum (again 71-dimensional descriptors). These target-focused clustering methods, which isolated targets and tagged them with individual spectra, were also compared with a layer-focused clustering method, which assigns averaged and simplified spectra to each depth/time bin, which is described below.

3.2.2. Clustering of averaged spectra

Ensemble-averaged acoustic-color scattering data were also used as 3-dimensional descriptors for the cluster analysis. For comparison with the target analyses described above, acoustic-color based clustering was first performed using the same 6-h dataset. It was then performed on the full Mar. 2008 to Feb. 2010 dataset.

For the 6-h dataset, the spectra from 30 pings (i.e. 30 s) were averaged before thresholding and converting to acoustic color as described in Section 3.1. For the two-year dataset, 1800 pings

(i.e. 30 min) were averaged before converting to acoustic color. To match the thresholding applied to the target spectra (where only targets with $S_V > -70$ dB were clustered), the mean pixel intensity was used to further threshold the data: only points with mean R–G–B pixel intensity greater than 0.25 (or $S_V > -70$ dB) were included in the cluster analysis of the 6-h dataset; however, as there were times in the two-year record when the total scattering in Saanich Inlet was weak relative to July 30, 2009, which resulted in too few retained bins to track the diel vertical migration (DVM), the threshold was relaxed to 0.1 (or -76 dB, 4 dB above the noise-level at the longest ranges) for the two-year record. After this thresholding, the R–G–B spectra were normalized by subtracting the largest R–G–B pixel intensity from each observation, which is equivalent to the normalization performed for the target spectra; the clustering was not sensitive to the choice of normalizing by the mean, minimum or maximum S_V .

An example of an acoustic color image from data collected on July 30, 2009 is shown in the bottom panel of Fig. 2. The upper left panel of Fig. 2 shows the normalized acoustic color similar to what was used in the clustering analysis. The upper right panel shows the minimum S_V in each bin. Adding the R–G–B values of the two upper panels yields the bottom panel, which contains both intensity and color information. Note that our narrow frequency range (85–155 kHz), across which most zooplankton scatter more strongly at higher frequencies (i.e., have 'blue spectra'), results in a low color range in our data; including higher frequencies would likely increase the range of colors in the spectra observed.

3.3. Net samples

As part of the Marine Bioacoustics course at Friday Harbor Laboratories, University of Washington, zooplankton net samples were collected near the broadband sonar in Saanich Inlet on July 30, 2009, using a 335 μm mesh, 0.25 m^2 MultiNet Plankton Sampler equipped with 5 nets, an electronic flowmeter and a CTD sensor towed at 3–4 knots. Stratified oblique zooplankton tows were conducted during the day, at dusk and during the night. Samples were fixed in 5% buffered formalin for later processing. The depth range for each net was chosen to target scattering layers observed with a vessel-mounted SIMRAD split beam ES-60 (38 and 120 kHz) and a pole-mounted split beam EK-60 (200 kHz) echosounders. The boxes in Fig. 2 show the depths and times of the dusk ($48^\circ 38.0456$ N, $123^\circ 30.4462$ W) and night-time ($48^\circ 39.378$ N, $123^\circ 30.389$ W) net samples. An equipment malfunction prevented use of the daytime samples. The net samples indicated in magenta in Fig. 2 were analyzed for zooplankton taxonomic- and size-composition. They were first split depending on numbers in the sample and then sorted into 9 taxonomic groups and counted. The lengths and widths of up to the first 50 individuals in each taxonomic group were measured.

3.3.1. Net samples: scattering predictions

The contribution to acoustic scattering from each taxonomic group in the nets was calculated using zooplankton scattering models described in Lavery et al. (2007). All groups, except shelled pteropods and siphonophore pneumatophores, were modeled as fluid-like shapes (uniformly bent-cylinders and prolate spheroids, see Lavery et al., 2007) using the distorted-wave Born approximation. Pteropods were modeled as spherical fluid-filled elastic shells and the single siphonophore pneumatophore was modeled using a hybrid gas-filled sphere model that accounts for damping near the bubble resonances (Lavery et al., 2007). In all cases the measured distribution of lengths and widths, along with Lavery et al.'s parameterization of the distribution of animal orientations and the density and sound speed contrasts, were used to make forward predictions of scattering cross-section per unit volume as a function of frequency.

4. Results

4.1. Sensitivity to pulse compression with clipped transmit pulse

Using the synthetic return and performing pulse compression using the synthetic transmit pulse clipped at different levels showed that there was no difference between using a transmit pulse clipped

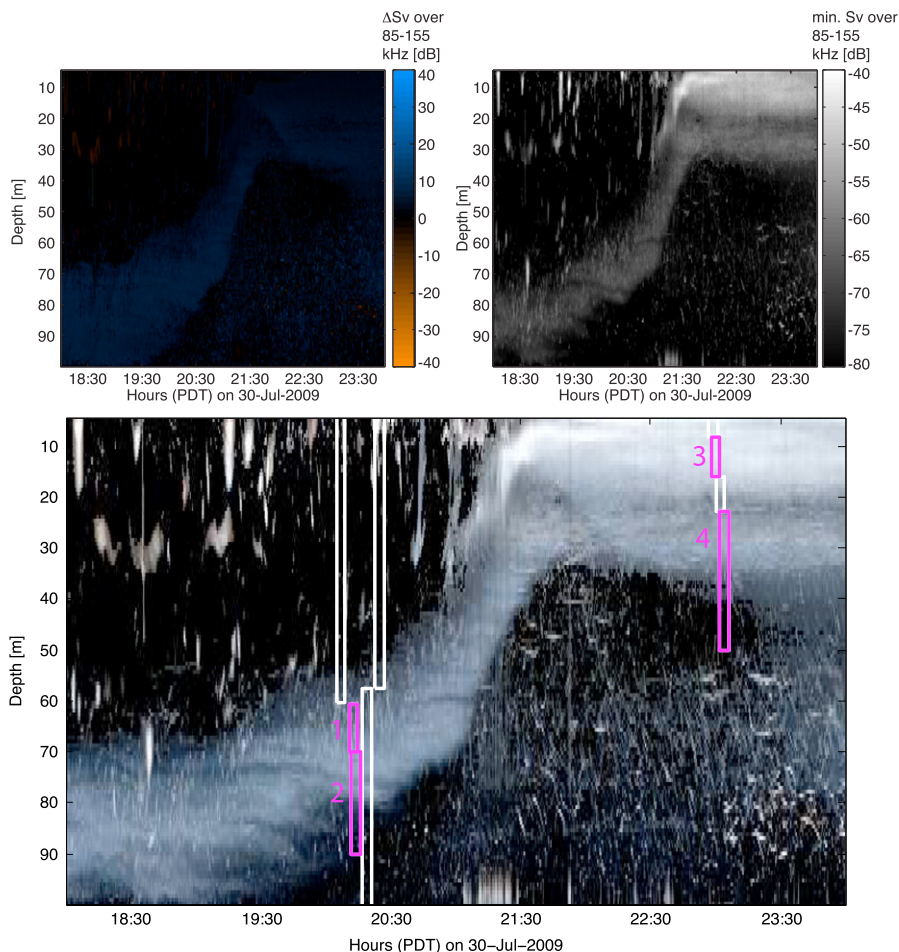


Fig. 2. Acoustic color representation of SciFish 85–155 kHz broadband acoustic data collected in Saanich Inlet on July 30, 2009. Top left: normalized color for each depth/time bin; the top left color bar indicates how a linear slope of the change in S_V over the 85–155 kHz band would color the bin. Top right: minimum intensity for each depth/time bin. Bottom: acoustic color image for the July 30, 2009 acoustic data created by the addition of the upper two panels (intensity and color). The white and magenta boxes indicate the approximate times and the depth ranges of zooplankton net tows conducted near the mooring site; magenta boxes indicate nets that were fully analyzed for species and size-composition.

at the 0.003% and 0.1% levels. Both showed a lower signal-to-noise improvement, about 85% of that of the unclipped transmit pulse (the full theoretical signal-to-noise improvement is $2WT = 140$, where W is the bandwidth and T is the length of the transmitted signal, [Chu and Stanton, 1998](#)).

When volume scattering strength was calculated using the synthetic, pulse compressed returns, the spectra calculated using the transmit pulses clipped at the 0.003% and 0.1% levels were again identical, but there was a 5–7 dB loss of sensitivity at the edges of the band (i.e. 85–90 kHz and 150–155 kHz). The spectra were also flatter and somewhat noisier than the one calculated with the unclipped transmit pulse (oscillations were about 2–3 dB larger for the clipped pulses). The change in shape of the spectrum should be compensated for by the fact that clipped transmit pulses were also used for the standard target calibration, but the noise seems to remain (see for instance the calibrated spectra in [Fig. 1](#) which all show a very similar pattern of spikes). The synthetic pulse analysis showed no difference between the 0.003% and 0.1% clipping levels, so the fact that the calibration data had to be collected with lower gain settings (in the 0.02–0.1% clipping range) should not affect the calibration.

Table 2

Numerical concentrations (N) and mean lengths (L , \pm standard deviation) of numerically and acoustically dominant zooplankton taxa found in the net samples indicated by the magenta boxes in Fig. 2. The water volume sampled by each net is given next to the net number. Euph = euphausiids; Chae = chaetognaths; Pter = pteropods; Amph = amphipods; Siph = siphonophores; Cope = copepods; Medu = medusae; Deca = decapods; and Crus = crustacean larvae.

Net	Vol.[m ³]		Euph	Chae	Pter	Amph	Siph	Cope	Medu	Deca	Crus
1	38	L[mm]	9 \pm 4	16 \pm 4	–	3 \pm 2	–	1.6 \pm 0.5	5 \pm 2	3.0 \pm 0.4	1.6 \pm 0.2
		N[m ⁻³]	67	59	–	5.5	–	190	5.9	3.8	3.8
2	164	L[mm]	9 \pm 6	11 \pm 4	–	3 \pm 2	2.8 [*] ,**	1.2 \pm 0.5	5 \pm 2	6 \pm 2	3 \pm 3
		N[m ⁻³]	21	28	–	16	0.098	270	0.88	0.78	3
3	68	L[mm]	7 \pm 4	15 \pm 4	2.1 [*]	2 \pm 1	1.9 \pm 0.3	1.5 \pm 0.4	6 \pm 1	–	4.1 \pm 0.3
		N[m ⁻³]	55	75	1.9	45	5.6	1200	0.1 ^{***}	–	7.5
4	222	L[mm]	9 \pm 3	14 \pm 4	2.4 \pm 0.4	3 \pm 2	4 \pm 2	1.4 \pm 0.3	4.5 \pm 0.6	5.4 \pm 0.9	–
		N[m ⁻³]	3.2	9.1	0.86	5.8	2.3	130	0.018 ^{***}	0.29	–

^{*} Only one organism in split.

^{**} This was a siphonophore pneumatophore (and was modeled as such in Fig. 3) all other siphonophore observations were of nectophores.

^{***} Entire sample counted.

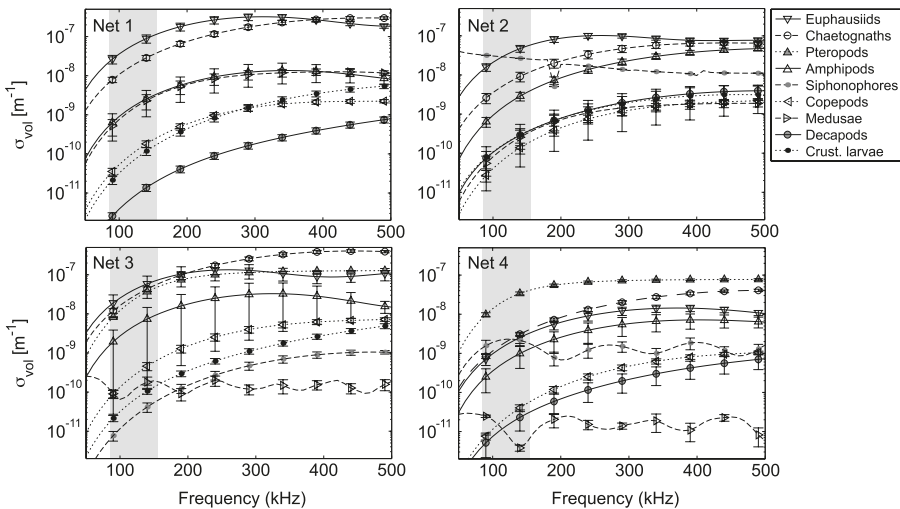


Fig. 3. Forward predictions of the scattering cross-section for each taxonomic group, based on typical estimates for distributions of orientation and sound speed and density contrasts as well as the measured sizes and concentrations, from the net samples indicated by magenta boxes in Fig. 2. The bandwidth of the SciFish sonar is indicated by the shaded region.

4.2. Net samples and scattering predictions

Table 2 shows the results of the analysis of the net samples indicated in magenta in Fig. 2. The size and abundance (based on split indicated in Table 2) of the main 9 taxonomic groups are tabulated.

The forward predictions of scattering cross-section per unit volume as a function of frequency for the main taxonomic groups found in the Saanich Inlet net samples are shown in Fig. 3.

As would be expected based on previous bioacoustical studies in Saanich Inlet, euphausiids are predicted to be the strongest scatterers in the 85–155 kHz band in the migrating layer (Nets 1 and 2; Fig. 3) and at the surface at night (Net 3). Pteropods are predicted to be the strongest scatterers in the net collected in the weaker scattering layer at 30 m depth during the night (Net 4). Chaetognaths are also strong contributors to the overall scattering, particularly at the surface at night (Net 3).

The total (i.e. summed) predicted volume scattering strength from each net (S_{Vpred} , seen in Fig. 4) was lower than the observed scattering strengths (S_{Vobs}). The frequency-averaged differences between

Table 3

Net-specific frequency-averaged differences between observed and predicted volume scattering strengths ($S_{Vdiff} = \overline{S_{Vobs}} - \overline{S_{Vpred}}$).

Net	S_{Vdiff} [dB]
1	12
2	10
3	27
4	18

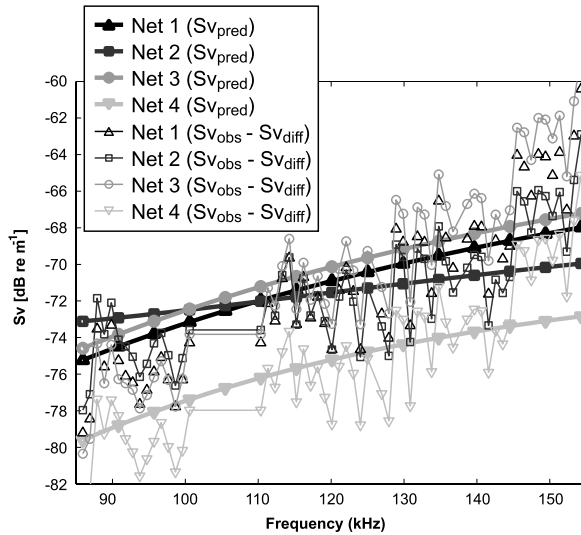


Fig. 4. A comparison of the observed and predicted total volume scattering strengths for each net. Each thick line is $10 \log_{10}$ of the sum of all the forward predictions for each net sample labeled in Fig. 2 (S_{Vpred}). The observed volume scattering strength averaged over the depth range of the net sample and ± 2 min around its time (S_{Vobs}) minus the frequency-averaged differences between observed and predicted scatterings (S_{Vdiff} ; Table 3), are shown with thin lines.

observed and predicted scattering ($S_{Vdiff} = \overline{S_{Vobs}} - \overline{S_{Vpred}}$; Table 3) are likely due to under-sampling of both large euphausiids and pteropods due to the net sampling methods. An experiment conducted in Saanich Inlet in July, 2011 found that scattering predictions based on net samples collected in the main euphausiid layer with strobe lights operating on a multiple opening/closing net system (Sameoto et al., 1993; Wiebe et al., 2004) agreed well with acoustic backscattering observations at 120 kHz (Marine Bioacoustics 2011, unpublished data). The forward predictions based on net samples collected in the main diel vertical migration (DVM) layer without strobe lights operating were consistently 5–15 dB lower than the observations (Marine Bioacoustics 2011, unpublished data). Pteropods are also known to be under-sampled by nets, as they can detect disturbances over 1 m away and escape at speeds of up to 45 cm/s (Lalli and Gilmer, 1989). Other possibilities for the disagreement are (1) lateral variability, as the nets did not sample the same water as the acoustics, (2) if the acoustics were mis-calibrated (i.e. if the calibration sphere was off-center), (3) if the beam volume was incorrectly estimated (however, both this and the previous would result in a constant offset across the nets), or (4) if fish were present in the layers. The frequency dependence of the total predicted volume scattering strengths is, however, consistent with the observations: in both the observations and predictions all of the layers have a blue hue and the slopes, or the linear trends to the frequency dependence, of the spectra agree well for each of the 4 nets (see $S_{Vobs} - S_{Vdiff}$ in Fig. 4), which suggests that the net predictions are a useful guide to interpreting the spectra if not the overall scattering levels.

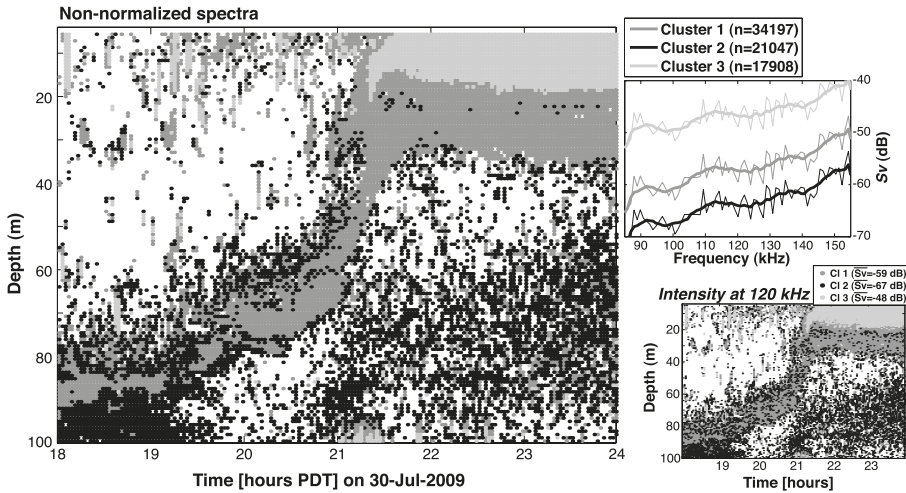


Fig. 5. Clustering result for July 30, 2009 18:00–24:00, using calibrated spectra (intensity and shape; left and top right panels) and the scattering intensity at 120 kHz (bottom right panel). The left panel shows the time and depth of each point that scattered above the threshold and the color indicates its clustering group based on the full calibrated spectra. The upper right panel shows the mean spectrum (i.e. the centroid) of each cluster. The thick lines are the same spectra smoothed using a 10 Hz running average across the spectrum. The bottom right panel is as for the left panel but with clusters based on the scattering intensity at 120 kHz alone (the cluster centroid S_V for each cluster is indicated in the legend).

4.3. Clustering based on target spectra

When clustering was performed using the non-normalized individual target spectral descriptors, three clusters were identified (Fig. 5). They all have similar slopes and are only differentiated by overall scattering strength. The grouping of the scattering observations was dominated by the overall level of the spectra, such that spatial/temporal distribution of the cluster results looks virtually identical when the clustering was done using only the individual target S_V at 120 kHz (bottom right panel of Fig. 5).

When clustering was performed using the normalized individual target spectral descriptors (Fig. 6), 4 distinct spectral shapes were identified: two that increased with frequency (i.e. would appear blue in the acoustic color plot; clusters #1 and #3), one that was nearly flat (i.e. would appear white or gray; cluster #2) and one that decreased with frequency (i.e. would appear red; cluster #4).

4.4. Clustering based on averaged acoustic-color spectra

Clustering based on acoustic color distinguished 4 clusters (Fig. 7) in the July 30, 2009 18:00 to 24:00 data. Only the normalized R–G–B pixel intensities (Fig. 7, lower right panel) were used as descriptors for the analysis, but the corresponding un-normalized cluster average R–G–B intensities and cluster average spectra are shown in Fig. 7 (upper right panel) to help interpret the clusters in terms of the expected scattering groups. Performing the same analysis on the July 30 data, but with 30 min (1800 ping) averaging instead of 30 s (30 ping) averaging (as in Fig. 7), while much coarser temporally, also yielded 4 clusters with very similar slopes and spatial–temporal distribution.

The cluster analysis of the two-year time series, with 30 min averaging, again distinguished 4 clusters (Fig. 8). A plot of the full water-column time series of the cluster results for this long time series is very difficult to read, because each diel period is extremely compressed, so the cluster results were pooled by month to highlight the variation in how often members of a particular cluster were observed seasonally and interannually (Fig. 8, left panel). The diel pattern in mean depth and frequency of observation of members of each cluster was highlighted by pooling the observations by time of day and calculating the mean depth of all members of the same cluster within the same hour (Fig. 8, bottom right panel).

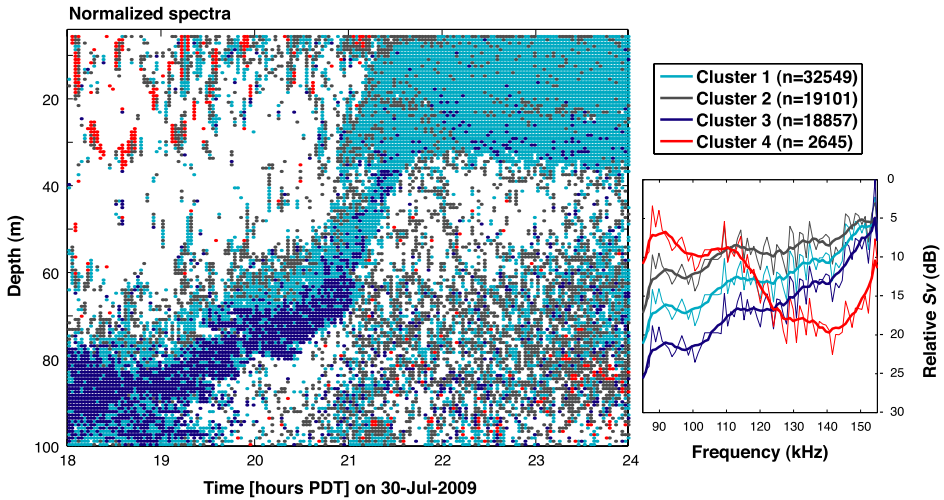


Fig. 6. Clustering result for July 30, 2009 18:00–24:00, using only spectral shape. The left panel shows the time and depth of each point that scattered above the threshold and the color indicates its clustering group. The right panel shows the mean spectrum (i.e. the centroid) of each cluster. The thick lines are the same spectra smoothed using a 10 Hz running average across the spectrum.

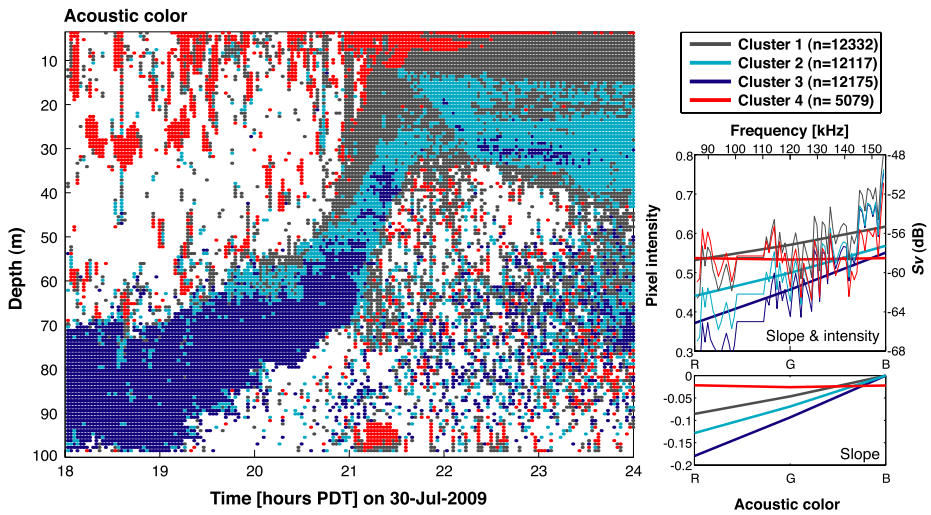


Fig. 7. Clustering result for July 30, 2009 18:00–24:00, using acoustic color data. The normalized R–G–B pixel intensities were used as a 3-dimensional descriptor of each point and only points with $S_v > -70$ dB were analyzed. The left panel shows the time and depth of each point and the color indicates its clustering group. The upper right panel shows the mean spectrum (i.e. the centroid) of each cluster, in both full 71-frequency (thin lines, right axis labels) and R–G–B (thick lines, left axis labels) forms. The lower right panel shows the normalized R–G–B cluster-centroid spectrum for each cluster.

5. Discussion

5.1. Importance of normalizing scattering spectra

Given the way the clustering distance criteria was formulated, the similarity between the clustering of non-normalized spectra and 120 kHz single-frequency data was no surprise. Since there was a large range of spectral levels relative to the range of spectral shapes, the absolute difference in the

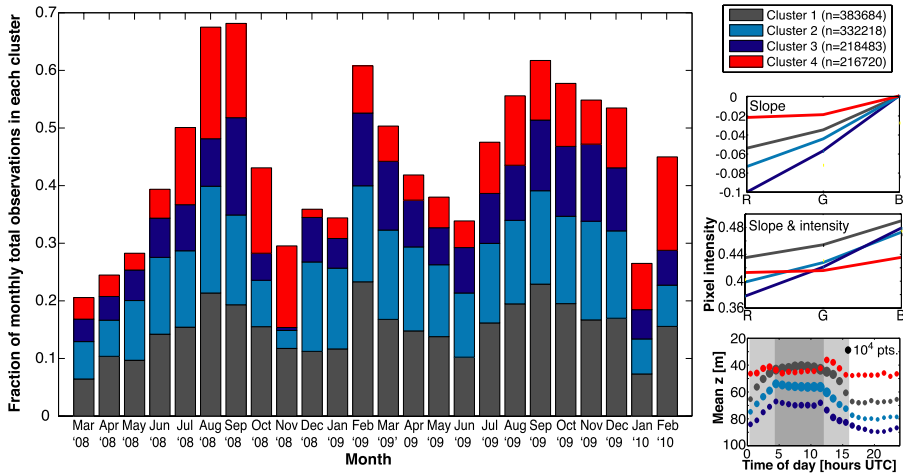


Fig. 8. Clustering result for March 2008 through February 2010 using acoustic color data. The normalized R–G–B pixel intensities were used as a 3-dimensional descriptor of each point. The left panel shows a histogram of the fraction of monthly observations that were classified in a given cluster. The stacked bars sum to the fraction of total observations with \bar{S}_v greater than -76 dB in that month. Shorter bars indicate months in which the total scattering in the water column was weaker. The upper and middle right panels show the mean cluster-centroid normalized and the corresponding un-normalized R–G–B pixel intensities, respectively. The lower right panel shows the mean (cluster-centroid) depth of the cluster as a function of time of day. The size of the circles indicates the total number of observations classified in that cluster in that hour over the entire 2 years. Note that the time is now given in UTC rather than local time (-8 h for PST and -7 h for PDT), which ensures consistency between seasons. Night-time is indicated by the shaded region in the bottom right panel; dark gray for hours that are dark year-round and light gray for hours that are dark seasonally.

non-normalized curves was a stronger driver for clustering than the shape of the spectra. Comparison of Figs. 2 and 5 shows that clustering based on the non-normalized spectra yields what one would expect based on grouping the observations by intensity. While very inefficient, because clustering a 71-point descriptor takes substantially more effort than a 1-point descriptor, it validates the idea that clustering based on spectra can successfully pick out the dominant variance. In this case the dominant variance was the overall scattering intensity, and thus many different spectral shapes are averaged within each cluster, leading to cluster-mean spectra that are nearly identical in shape. The noise (or bumps on the spectra) were similar for all observed spectra and were related to noise in the system (introduced in part due to using clipped transmit pulses), which is why we plotted smoothed spectra as well (thick lines in upper right panel of Fig. 5). These intensity based groupings contain no frequency-dependent scattering information and are therefore subject to the normal ambiguities in interpreting single-frequency acoustic data; many small organisms can scatter as strongly as few larger organisms.

Cluster #1 in Fig. 5, the mid-intensity middle gray spectrum, represents what the nets suggest was a euphausiid-dominated diel vertical migration (DVM) layer before dusk and the pteropod-dominated layer below the euphausiid-dominated layer after dusk (Nets 1, 2 and 4; Figs. 2 and 3). Cluster #2 in Fig. 5 represents part of the daytime euphausiid-dominated DVM layer and the unknown 60–90 m community at night. Cluster #3 in Fig. 5, the highest intensity light-gray spectrum, represents the night-time euphausiid and chaetognath dominated layer (Net 3; Figs. 2 and 3) as well as what was likely fish schools in the upper water column during the day. All are combinations of the observed biological assemblages, which was no surprise because the groupings are intensity dominated (meaning that the groups can only be interpreted at the net locations).

Conceptually, better differentiation between groups can be achieved by removing the intensity signal and clustering based on spectral shape alone. Scattering models predict that different sizes of zooplankton will have different frequency dependences to their scattering, and size can be a fairly good indicator of taxonomic group (especially in a relatively simple system like Saanich Inlet, e.g. Bary et al., 1962, and Table 2). Using shape alone (i.e. normalizing such that the peak of each spectrum is at

$S_V = 0$), allows size to become the dominant distinguishing factor. A large number of small scatterers can produce the same volume scattering strength as a small number of large scatterers, but they will not have the same spectral shape. As discussed in detail in the following subsection, clustering based on the normalized spectra results in a better identification of biologically meaningful layers. The results were nearly identical if other normalization methods, such as removing the mean or minimum S_V from each spectrum, were used. This indicates that the analysis is not sensitive to the normalization method: the key is to remove the effect of the strong variability in the overall scattering level to focus the clustering on frequency-dependent differences.

5.2. Normalized, target-based clustering

When the spectra were normalized before clustering, there were four clusters identified. Cluster #4 in Fig. 6, with a decreasing (i.e. red) spectrum and the fewest members, was associated primarily with what are presumably fish schools in the water above the migrating layer. The frequency dependence of these schools was predominantly a beam angle effect: the beam is wider in the lowest frequencies, so a school passing across the beam will appear first at the lower frequencies, making the edges of the school scattering patches red (see Fig. 2). They often have gray or light blue centers. These flatter spectral shapes (clusters #1 and #2 in Fig. 6, appearing light blue and gray respectively) were much more common and were predominantly associated with the night-time near surface scattering (euphausiid and chaetognath dominated in the nets) and the deep night-time layer (unsampled composition) as well as the edges of the daytime deep layer (also euphausiid and chaetognath dominated in the nets). The only zooplankton in the nets that are predicted to have spectra as flat as cluster #2 in Fig. 6 were siphonophores and medusae (though medusae are predicted to be quite weak scatterers). It is also likely, however, that larger euphausiids were preferentially missed by the nets (e.g. Wiebe et al., 2004) and cluster #2 may also be populated by scattering observations from large euphausiids (which would have flatter spectra). The spectral slopes of clusters #1 and #3 in Fig. 6 (appearing light and dark blue in acoustic color images) are consistent with most of the other species observed in the nets (i.e. comparing Figs. 3 and 6). Note that while copepods were very abundant in many of the nets (particularly Net 3) they are unlikely to have much effect on even the normalized cluster results if they occupy the same space as the larger organisms because the larger organisms scatter much more strongly in the 85–155 kHz band (Fig. 3).

The distinction between clusters #1 and #3 appears to have less meaning in terms of species composition. Cluster #3 appears to migrate to the surface and become cluster #1. As the DVM layer is a group which would clearly have the largest number of members (given the thresholding to retain only targets with $S_V > -70$ dB), this splitting of the DVM layer into two clusters may result from the bias of the k -means method towards creating equally-sized clusters. However, though strongly euphausiid influenced, the forward predictions based on Nets 1, 2 and 3 (Fig. 3) suggest that there is a shift toward higher scattering contribution from larger chaetognaths and pteropods in the night-time DVM layer. Thus, the different classification does perhaps reflect a real change in the type of targets observed.

While the normalized clustering is better able to distinguish fish spectra from zooplankton spectra than the non-normalized version, it still does not make a strong distinction between the two different night-time layers seen in the nets. Observations from both the surface euphausiid and chaetognath dominated layer and the pteropod-dominated layer beneath it are mostly classified as cluster #1 in Fig. 6. There are, however, more observations classified as the flattest (cluster #2) within the upper layer and more observations classified as the steepest increasing (cluster #3) within the lower layer, suggesting that, in the aggregate, the method makes some distinction between the layers. The problem may lie in the idea of characterizing each layer by a single dominant organism. Each layer has a different assemblage of organisms. A better way of identifying layers may be by the mean frequency-dependence of the assemblage, which suggests that ensemble-averaging of single-ping spectra may help in distinguishing between and classifying layers (i.e. replace the speckling pattern seen in Fig. 6 with two different clusters based on the assemblage).

This leads to the idea that the clustering method can be made more efficient. First, averaging over multiple pings will better represent the ensemble of observations in a layer (making the observational

data more consistent with the ensemble averaging assumed in zooplankton scattering models). The frequency of speckles in the night-time near surface layers in Fig. 6 suggests that averaging over 15–30 min may be necessary, though perhaps adjacent depth bins could also be averaged. Second, for the normalized spectra, which could broadly distinguish between scattering groups, the shapes of the cluster-centroid spectra mainly differed in their slope. Thus, a 3-point spectrum (like the R–G–B spectrum of the acoustic color data) would be sufficient to retain the broad shape parameters useful for discrimination and comparison with scattering models. While a 2-point spectrum could represent the slope, a 3-point spectrum is better placed to resolve any Rayleigh-to-geometric transition that might occur in the 85–155 kHz band.

5.3. Focus on layer averages: more efficient clustering

The acoustic color clustering of the July 30, 2009 18:00 to 24:00 data (Fig. 7) did a much cleaner job of distinguishing the scattering layers than the normalized, target-spectrum analysis. Again, a cluster with scattering strength that decreases with increasing frequency (i.e. appearing red, cluster #4 in Fig. 7) appears to be associated with fish schools near the surface before sunset. As discussed above, the spectral shape is likely due to the frequency-dependent beamwidth effect. Also similar to the normalized, target-spectrum result, the cluster with the steepest increasing spectrum (i.e. appearing strongly blue, cluster #3 in Fig. 7) occupied the earlier part of the record, when the dominant scattering layer was close to the bottom. However, in this result, there were two distinct layers in the night-time near surface scattering (clusters #1 and #2 in Fig. 7).

In Fig. 7, as the DVM layer migrated to the surface, its scattering spectrum became less steep: first cluster #3 (appearing strongly blue blue), then cluster #2 (appearing weakly blue), then cluster #1 (appearing gray). Based on the net tows, clusters #1 and #3 likely represent the euphausiid and chaetognath dominated scattering layer at different stages of its DVM. The spectral slope of cluster #2 is steeper than cluster #1, but flatter than cluster #3. Cluster #2 likely represents the transition of cluster #3 to cluster #1 during DVM. At night, however, cluster #2 sat about 15 m below the strong surface scattering layer represented by cluster #1. The net sample collected in that layer suggested a zooplankton assemblage with acoustic scattering dominated by pteropods (Net 4, Fig. 3). Whereas the upper layer (cluster #1 in Fig. 7; Net 3 in Fig. 3) had similar scattering from pteropods but also equally high levels of scattering from both chaetognaths and euphausiids. Copepods and small amphipods were also quite abundant in Net 3, but are weaker scatterers, so are less likely to affect the clustering result. These additional species, found in much higher numbers in Net 3 as compared to Net 4, may be aggregated at the surface to feed at night. Given this biological distinction between Nets 3 and 4 and that most of the points classified as cluster #2 (Fig. 7) occurred at night, cluster #2 most likely represents a distinct biological layer with pteropod-dominated scattering. The fact that it sometimes represents layers with scattering dominated by other taxonomic groups is a reflection of both the inherent ambiguity of trying to classify this set of organisms with a limited frequency bandwidth (see Fig. 3) and the bias of *k*-means clustering towards equally-sized clusters.

Based on what is known from the net samples, this method, averaging over many pings and using a simplified representation of the scattering spectra, appears to come the closest to distinguishing between the dominant scatterers in the water column of Saanich Inlet on July 30, 2009. Too many clusters were identified, with the DVM scattering layer being classified as a separate group during the day and night. This appears, however, to be the result of a real difference in spectral shape, perhaps reflecting a different species composition during the day (note that some of cluster #1 remains at depth during the night and the predictions based on the nets showed a larger scattering contribution from chaetognaths at night, Fig. 3) or a change in the mean size (e.g. De Robertis, 2002; Tarling, 2003) and/or orientation (e.g. Simard and Sourisseau, 2009) of the acoustically-dominant euphausiid population.

5.4. Clustering two years of observations

Of more direct applicability to the analysis of observatory-based acoustic observations is testing the ability of the acoustic color clustering method to distinguish the dominant biological scattering layers in a much longer record (Fig. 8). Multi-year observation periods, where there will only be sparse

coincident net samples available to validate the scattering data, are typical of observatories. The full March 2008 through February 2010 Saanich Inlet dataset was not continuous, as the sonar needed to be stopped to upload data and was recovered for a brief servicing every 6 months. However, there were data from enough diel periods in each month to give a good representation of monthly changes in the total scattering and the clusters present. There appears to be a seasonal cycle in total scattering, with the strongest scattering in late summer/early fall and a secondary peak in February (Fig. 8).

Due to the sparsity of net-samples to compare with, much of the inference of the biological composition of the clusters in the long-term data comes from comparing the patterns of the clusters, e.g., depth distribution over daily and seasonal cycles, with previously reported observations of organisms in Saanich Inlet (as well as the spectral slopes expected for the dominant organism in each group). Again, four clusters were identified and some of them appear to be linked: some appear much more frequently at night and others during the day (Fig. 8). For example, in terms of numbers of observations clusters #1 and #3 are out of phase on the diel cycle, but roughly in phase on the annual cycle. Examination of the full water-column time series plot (not shown, but similar to the left panel of Figs. 5–7) show that they often represent the day (#3) and night (#1) of the DVM scattering layer. As with the July 30-only result (Fig. 7), these are likely euphausiid-dominated scattering layers. Euphausiids are known to be present in Saanich Inlet in all seasons (e.g. Bary et al., 1962) and exhibit a strong DVM with much higher concentrations and thus stronger scattering in the night-time surface layer. Also, as with the July 30-only result, the day-time at-depth DVM scattering layer (i.e. cluster #3) has a steeper spectral slope in Fig. 8. At times this layer was also present at night, though generally spread throughout the water column below the main DVM layer.

Cluster #2 in Fig. 8 shows a similar diel cycle to cluster #1, but in the full water-column time series plot only cluster #1 consistently represents the main, full water column, DVM. When we examined just July 30, 2009 in the full water-column time series plot for the full two years (not shown but referring to the clusters summarized in Fig. 8), we observed that the two-year cluster #2 was distributed in almost exactly as cluster #2 in the July 30-only result (seen in Fig. 7) in this case representing the transitional (i.e. migrating) stage of the DVM and settling 10–20 m below the main DVM. This was observed on many other occasions. However, on many nights in the full water-column time series plot for the full two years (not shown), the entire water column beneath the main DVM layer was filled with scattering observations grouped into cluster #2. Other times, cluster #2 represented a separate scattering layer that appeared only at night at mid-depths. Cluster #2 is therefore harder to associate with a single zooplankton assemblage, seeming to alternate between representing a pteropod-dominated layer that migrates near to the surface at night (as in the July 30, 2009 data) and a layer that migrates from below the echosounder into the water column at night. This latter behavior suggests that cluster #2 sometimes represents an amphipod-dominated layer. Amphipods have been observed to have a large standing stock in Saanich Inlet that in most seasons migrates from the anoxic benthos into oxic waters above (De Robertis et al., 2001). Although not in Saanich Inlet, amphipods have been observed to migrate on a diel cycle (Kaartvedt, 1986). This is consistent with cluster #2, which was rarely observed during the day (when the amphipods were presumably on the bottom).

Cluster #4 in Fig. 8, with its relatively high intensity, quite flat spectral shape and near surface day-time presence, likely represents fish schools (as seen in the daytime surface waters on July 30, 2009, Figs. 6 and 7). It appears, however, to also at times represent the night-time surface DVM layer. This is true on July 30, 2009 in the two-year results; the night-time surface scattering layer (i.e. everything assigned to cluster #1 in Fig. 7) is assigned to cluster #4 above 12 m and the portion between 12 and 20–25 m is assigned to cluster #1. The subsurface scattering layer is assigned to cluster #2 in the two-year results, consistent with the July 30-only results. Also consistent with the July 30-only results, cluster #3 in Fig. 8 represents the DVM layer at depth during the day (cluster #3 in Fig. 7) and cluster #4 in Fig. 8 is assigned to the likely-fish scattering seen in the surface waters before dusk (cluster #4 in Fig. 7). The fact that cluster #4 in the two-year result is assigned at times to the surface DVM layer as well as scattering from fish schools is likely why its spectral slope does not decrease with increasing frequency (i.e. red spectrum due to frequency-dependent beamwidth effects) as in the July 30-only result. Cluster #4 was observed more frequently in late summer and fall, which is consistent with previous observations of high concentrations of fish in the fall (Herlinveaux, 1962).

The association of clusters #2 and #4 with more than one group may be a consequence of changes in the frequency-dependence of the different assemblages, either through changes in the size distribution (through growth and immigration/emigration) or species composition, that overlap between groups (e.g. euphausiids and chaetognaths in the July 30 data). For instance, juvenile euphausiids might be indistinguishable in frequency response from mature pteropods, so, although they appear in different seasons, they may cluster together. We do not have sufficient supporting data (net samples, for example) to distinguish between this type of clustering error, based on insufficient descriptors, and failure of the *k*-means as a clustering technique. The *k*-means technique is biased toward creating equally-sized clusters and cannot distinguish between groups that overlap in their distribution (like our speculated overlap between the frequency-dependence of juvenile euphausiids and mature pteropods).

6. Conclusions

With the zooplankton species present in Saanich Inlet, B.C., the combination of simplifying the 85–155 kHz broadband spectra into acoustic color data and then applying a simple *k*-means clustering method on the normalized spectra appears to be the most efficient way of distinguishing between biological scattering layers. Both steps reduce the volume of data handled, which is a benefit for high data volume operations such as ocean observatories, while retaining the essential spatial and frequency-dependent scattering information to maximize the interpretation of scattering layers.

Normalizing the spectra was key to taking advantage of the frequency-dependence of the scattering as a means of distinguishing both targets and layer-specific assemblages of zooplankton. The clustering of the non-normalized spectra resulted in clusters dominated by the frequency–mean scattering intensity, and was therefore subject to the normal ambiguities in interpreting single-frequency acoustic data; many small organisms can scatter as strongly as few larger organisms. While the normalized target spectra clusters did a better job of separating different types of scatterers, the results were still difficult to interpret because (1) they did a poor job of identifying scattering layers (likely due to the mixed assemblages) and (2) the organisms present had scattering spectra that were too similar within the 85–155 kHz range to fully distinguish them.

Averaging and simplifying the spectra improved the consistency of the classification within layers, making the results easier to associate with biological groupings. It appears that although the individual targets' normalized scattering spectra are difficult to distinguish, summing the scattering spectra of the members of the different assemblages in each layer yields normalized scattering spectra that can be distinguished using the 85–155 kHz band.

Even with averaging, the classification of layer-specific assemblages of zooplankton was imperfect, sometimes putting what were likely (based on net tows and what is known about a group's behavior) two distinct groups in the same cluster or splitting what appeared to be a single group (i.e. the main DVM layer) into 2 clusters, though the latter may reflect different assemblages in the daytime and nighttime DVM layer. This is inconvenient when the goal is to automate the classification of layers in the long-term acoustic datasets coming from observatories. The frequency-dependence is sensitive to the size of the organisms, which, while useful in distinguishing taxonomic groups, cannot distinguish between zooplankton groups of similar size (for instance, pteropods and amphipods, Fig. 3). Thus, it may be necessary to include more descriptors, such as a measure of depth as a function of time-of-day, to isolate layers dominated by organisms of similar sizes but different behaviors.

Based on the previous observational studies in Saanich Inlet, the layer classification resulting from the clustering of the two-year dataset is likely a reasonable representation of the acoustically dominant organisms in Saanich Inlet. Four clusters were identified that distinguished what were likely four biological groups dominated by distinct organisms: fish, euphausiids, amphipods and pteropods. Unfortunately, amphipods and pteropods were mixed into a single cluster, likely due to similarities in size (Table 2 and Fig. 3). Euphausiids were classified into 2 clusters (day-time and night-time), which may represent a real change, either through a higher number of co-located chaetognaths at night (as on July 30, 2009), a change in mean orientation (e.g. Simard and Sourisseau, 2009) or size distribution (e.g. De Robertis, 2002; Tarling, 2003). Particularly in this long time series, having one cluster representing different groups at different times may also be a consequence of the tendency

of the *k*-means algorithm to produce equally-sized clusters regardless of whether the groups should be equally populated (Yan, 2005). An exploration of other blind-classification schemes that allow for unequally-sized clusters would be useful.

While long term acoustic observations are one of the best ways to examine the interannual variability in the dominant scattering groups, distinguishing these taxonomic groups without extensive supporting video or net-tow observations would likely benefit from higher-frequency observations to better monitor the smaller organisms and lower-frequency observations to better monitor fish. In Saanich Inlet, based on the July 30 data, extending the band to higher frequencies should provide better discrimination between zooplankton species, because most were still in the Rayleigh scattering regime in 85–155 kHz. Given the fact that the clustering analysis performed just as well with simplified spectral information, the most efficient way of extending the band might be to use a multi-frequency narrow band sonar system, since the data volume associated with multiple broadband systems could be prohibitive. For observatories outside of a Saanich Inlet like system, whether a multi-frequency narrow-band or broadband system would be most beneficial will depend on the types of scatterers present. Accurate frequency resolution can be important for the identification of some groups (e.g. fish with swim bladder resonances, Stanton et al., 2010).

Acknowledgments

We are grateful to Richard Dewey, Paul Macoun and the rest of the VENUS team for making the SciFish sonar work nearly seamlessly for two years. We thank Charles Greene and all the participants of the 2009 and 2011 Marine Bioacoustics course at Friday Harbor Laboratories for collecting and sharing net-tow data and analysis from Saanich Inlet. In particular, we acknowledge the contributions of Wu-Jung Lee, a student in the 2009 Marine Bioacoustics course who provided Matlab code which applied *k*-means clustering to broadband volume backscattering data to facilitate this study.

Appendix. Supplementary data

Supplementary material related to this article can be found online at <http://dx.doi.org/10.1016/j.mio.2013.05.001>.

References

- Anderson, C.I.H., Horne, J.K., Boyle, J., 2007. Classifying multi-frequency fisheries acoustic data using a robust probabilistic classification technique. *J. Acoust. Soc. Am.* 121 (6), EL230–237.
- Anderson, J.J., Devol, A.H., 1973. Deep water renewal in Saanich Inlet, an intermittently anoxic basin. *Estuar. Coast. Mar. Sci.* 1 (1), 1–10.
- Bary, B.M., Barraclough, W.E., Herlinveaux, R.H., 1962. Scattering of underwater sound in Saanich Inlet, British Columbia. *Nature* 194, 36–37.
- Boden, B.P., Kampa, E.M., 1965. An aspect of euphausiid ecology revealed by echo-sounding in a fjord. *Crustaceana* 9 (2), 155–173.
- Brundage, H., Jung, J.B., 2009. Experiments with broadband sonar for the detection and identification of endangered shortnose sturgeon. *MTS Journal* 43 (3), 78–82.
- Burgos, J.M., Horne, J.K., 2008. Characterization and classification of acoustically detected fish spatial distributions. *ICES J. Mar. Sci.* 65, 1235–1247.
- Chu, D., Stanton, T., 1998. Application of pulse compression techniques to broadband acoustic scattering by live individual zooplankton. *J. Acoust. Soc. Am.* 104, 39–55.
- Cox, M.J., Watkins, J.L., Reid, K., Brierley, A.S., 2011. Spatial and temporal variability in the structure of aggregations of Antarctic krill (*Euphausia Superba*) around South Georgia, 1997–1999. *ICES J. Mar. Sci.* 68 (3), 489–498.
- De Robertis, A., 2002. Size-dependent visual predation risk and the timing of vertical migration: an optimization model. *Limnol. Oceanogr.* 47 (4), 925–933.
- De Robertis, A., Eiane, K., Rau, G.H., 2001. Eat and run: anoxic feeding and subsequent aerobic recovery by orchemone obtusus in Saanich Inlet, British Columbia, Canada. *Mar. Ecol. Prog. Ser.* 219, 221–227.
- De Robertis, A., Jaffe, J.S., Ohman, M.D., 2000. Size-dependent visual predation risk and the timing of vertical migration in zooplankton. *Limnol. Oceanogr.* 45 (8), 1838–1844.
- Dewey, R., Tunncliffe, V., Round, A., Macoun, P., Vervynck, J., 2009. Venus: the Victoria experimental network under the sea. *CMOS Bulletin* 37 (3), 77–82.
- Faran, J.J., 1951. Sound scattering by solid cylinders and spheres. *J. Acoust. Soc. Am.* 23, 405–418.
- Friedman, H., Rubin, J., 1967. On some invariant criteria for grouping data. *J. Amer. Statist. Assoc.* 62 (320), 1159–1178.

- Gan, G., Ma, C., Wu, J., 2007. Data Clustering: Theory, Algorithms, and Applications. In: ASA-SIAM Series on Statistics and Applied Probability. SIAM, Society for Industrial and Applied Mathematics.
- Gargett, A.E., Stucchi, D., Whitney, F., 2003. Physical processes associated with high primary production in Saanich Inlet. *British Columbia. Estuar. Coast. Shelf Sci.* 56, 1141–1156.
- Greenlaw, C.F., 1979. Acoustical estimation of zooplankton populations. *Limnol. Oceanogr.* 24 (2), 226–242.
- Herlinveaux, R.H., 1962. Oceanography of Saanich Inlet in Vancouver Island, British Columbia. *J. Fish. Res. Board Can.* 19 (1), 1–37.
- Holliday, D.V., 1977. Extracting bio-physical information from the acoustic signatures of marine organisms. In: *Oceanic sound scattering prediction*. Plenum Press, pp. 619–624.
- Horne, J.K., 2000. Acoustic approaches to remote species identification: a review. *Fisheries Oceanography* 9 (4), 356–371.
- Intrator, N., Neretti, N., Huynh, Q., 2004. Sonar object discrimination via spectral density analysis. In: *OCEANS '04 MTS/IEEE Techno-Ocean '04 Conference Proceedings*. vol. 2. IEEE/MTS, USA, pp. 740–742. IEEE, 345 E 47th St, New York, NY 10017.
- Kaartvedt, S., 1986. Diel activity patterns in deep-living cumaceans and amphipods. *Mar. Ecol. Prog. Ser.* 30, 243–249.
- Lalli, C.M., Gilmer, R.W., 1989. *Pelagic Snails: The Biology of Holoplanktonic Gastropod Mollusks*. Stanford University Press, Stanford, California.
- Lavery, A.C., Chu, D., Moum, J.N., 2010. Measurements of acoustic scattering from zooplankton and oceanic microstructure using a broadband echosounder. *ICES J. Mar. Sci.* 67, 379–394.
- Lavery, A.C., Wiebe, P.H., Stanton, T.K., Lawson, G.L., Benfield, M.C., Copley, N., 2007. Determining dominant scatterers of sound in mixed zooplankton populations. *J. Acoust. Soc. Am.* 122 (6), 3304–3326.
- Lawson, G.L., Wiebe, P.H., Stanton, T.K., Ashjian, C.J., 2008. Euphausiid distribution along the Western Antarctic Peninsula—Part A: Development of robust multi-frequency acoustic techniques to identify euphausiid aggregations and quantify euphausiid size, abundance, and biomass. *Deep-Sea Res. I* 55, 412–431.
- Lee, W.-J., July 2009. Target discrimination and classification using broadband acoustic techniques — Saanich Inlet: a case study, final project report for 2009 Friday Harbor Laboratories Marine Bioacoustics course.
- Mackie, G., Mills, C.E., 1983. Use of the Pisces IV submersible for zooplankton studies in coastal waters of British Columbia. *Can. J. Fish. Aquat. Sci.* 40, 763–776.
- MacQueen, J., 1967. Some methods for classification and analysis of multivariate observations. In: *Lecam, L., Neyman, J. (Eds.), Proceedings of the Fifth Berkeley Symposium on Mathematical Statistics and Probability*. vol. 1. University of California Press, Berkeley and Los Angeles, California, pp. 281–297.
- Miklovic, D.W., Bird, M.T., 1998. Quantitative acoustic color displays for classification with broadband sonars. In: *OCEANS'98 — Conference Proceedings*. vol. 1. IEEE, USA, pp. 592–597. 345 E 47th St, New York, NY 10017.
- Preston, J., 2009. Automated acoustic seabed classification of multibeam images of Stanton Banks. *Appl. Acoust.* 70, 1277–1287.
- Roberts, P.L.D., Jaffe, J.S., 2007. Multiple angle acoustic classification of zooplankton. *J. Acoust. Soc. Am.* 121 (4), 2060–2070.
- Roberts, P.L.D., Jaffe, J.S., 2008. Classification of live, untethered zooplankton from observations of multiple-angle acoustic scatter. *J. Acoust. Soc. Am.* 124 (2), 796–802.
- Romaine, S.J., Mackas, D.L., Macaulay, M.C., 2002. Comparison of euphausiid population size estimates obtained using replicated acoustic surveys of coastal inlets and block average vs. geostatistical spatial interpolation methods. *Fisheries Oceanography* 11 (2), 102–115.
- Sameoto, D., Cochrane, N., Herman, A., 1993. Convergence of acoustic, optical, and net-catch estimates of euphausiid abundance: Use of artificial light to reduce net avoidance. *Can. J. Fish. Aquat. Sci.* 50, 334–346.
- Simard, Y., Sourisseau, M., 2009. Diel changes in acoustic and catch estimates of krill biomass. *ICES J. Mar. Sci.* 66, 1318–1325.
- Stanton, T.K., Chu, D., Wiebe, P.H., Martin, L.V., Eastwood, R.L., 1998. Sound scattering by several zooplankton groups. I. Experimental determination of dominant scattering mechanisms. *J. Acoust. Soc. Am.* 103, 236–253.
- Stanton, T.K., Chu, D., 2008. Calibration of broadband active acoustic systems using a single standard spherical target. *J. Acoust. Soc. Am.* 124, 128–136.
- Stanton, T.K., Chu, D., Jech, J.M., Irish, J.D., 2010. New broadband methods for resonance classification and high-resolution imagery of fish with swimbladders using a modified commercial broadband echosounder. *ICES J. Mar. Sci.* 67, 365–378.
- Tarling, G.A., 2003. Sex-dependent diel vertical migration in northern krill *meganctiphanes norvegica* and its consequences for population dynamics. *Mar. Ecol. Prog. Ser.* 260, 173–188.
- Tarling, G.A., Klevjer, T., Fielding, S., Watkins, J., Atkinson, A., Murphy, E., Korb, R., Whitehouse, M., Leaper, R., 2009. Variability and predictability of Antarctic krill swarm structure. *Deep-Sea Res. I* 56, 1994–2012.
- Trenkel, V.M., Ressler, P.H., Jech, M., Giannoulaki, M., Taylor, C., 2011. Underwater acoustics for ecosystem-based management: state of the science and proposals for ecosystem indicators. *Mar. Ecol. Prog. Ser.* 442, 285–301.
- Vagle, S., Foote, K.G., Trevorrow, M.V., Farmer, D.M., 1996. A technique for calibration of monostatic echosounder systems. *IEEE J. Ocean. Eng.* 21 (3), 298–305.
- Warren, J.D., Stanton, T.K., Wiebe, P.H., Seim, H.E., 2003. Inference of biological and physical parameters in an internal wave using multiple-frequency, acoustic-scattering data. *ICES J. Mar. Sci.* 60, 1033–1046.
- Wiebe, P.H., Ashjian, C.J., Gallager, S.M., Davis, C.S., Lawson, G.L., Copley, N.J., 2004. Using a high-powered strobe light to increase the catch of Antarctic krill. *Mar. Biol.* 144, 493–502.
- Yan, M., Methods of determining the number of clusters in a data set and a new clustering criterion. Ph.D. thesis, Virginia Polytechnic Institute and State University, 2005.